Physics of Plasmas

Collisionless magnetic reconnection in the presence of a guide field

Paolo Ricci, J. U. Brackbill, W. Daughton, and Giovanni Lapenta

Citation: Phys. Plasmas **11**, 4102 (2004); doi: 10.1063/1.1768552
View online: http://dx.doi.org/10.1063/1.1768552
View Table of Contents: http://pop.aip.org/resource/1/PHPAEN/v11/i8
Published by the American Institute of Physics.

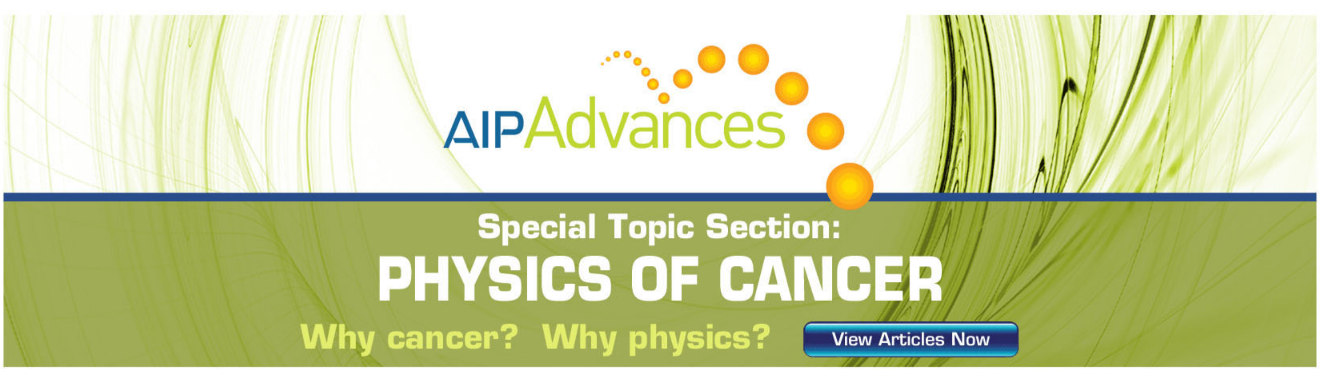

Collisionless magnetic reconnection in the presence of a guide field

Paolo Ricci[a)]
Istituto Nazionale per la Fisica della Materia (INFM), Unità del Politecnico di Torino, Corso Duca degli Abruzzi 24-10129 Torino, Italy and Dipartimento di Energetica, Politecnico di Torino, Torino, Italy

J. U. Brackbill[b)] and W. Daughton[c)]
Los Alamos National Laboratory, Los Alamos, New Mexico 87545

Giovanni Lapenta[d)]
Istituto Nazionale per la Fisica della Materia (INFM), Unità del Politecnico di Torino, Corso Duca degli Abruzzi 24-10129 Torino, Italy and Los Alamos National Laboratory, Los Alamos, New Mexico 87545

(Received 2 March 2004; accepted 12 May 2004; published online 20 July 2004)

The results of kinetic simulations of magnetic reconnection in Harris current sheets are analyzed. A range of guide fields is considered to study reconnection in plasmas characterized by different β values, $\beta > m_e/m_i$. Both an implicit particle-in-cell (PIC) simulation method and a parallel explicit PIC code are used. Simulations with mass ratios up to the physical value are performed. The simulations show that the reconnection rate decreases with the guide field and depends weakly on the mass ratio. The off-diagonal components of the electron pressure tensor break the frozen-in condition, even in low β plasmas. In high β plasmas, evidence is presented that whistler waves play a key role in the fast reconnection physics, while in low β plasmas the kinetic Alfvén waves are important. The in-plane and the out-of-plane ion and electron motion are also considered, showing that they are influenced by the mass ratio and the plasma β. *© 2004 American Institute of Physics.* [DOI: 10.1063/1.1768552]

I. INTRODUCTION

Magnetic reconnection causes global changes of the magnetic field topology and of the plasma properties, and the conversion of magnetic energy into plasma particle kinetic energy in form of plasma jetting and plasma heating.[1,2] It is observed to occur in collisionless plasmas over a wide range of β values: In the geomagnetic tail,[3] $\beta \gg 1$; the Earth's magnetopause,[4] $\beta \approx 1$; the solar corona,[2] laboratory[5,6] and fusion plasmas,[1] and astrophysical plasmas,[7] $\beta \leqslant 1$.

In the high β case, the geospace environment magnetic (GEM) reconnection challenge (see Ref. 8 and references therein) has clarified the physics of fast reconnection. The primary mechanism by which the frozen-in condition is broken is given by the nongyrotropic electron pressure terms (e.g., see Refs. 9 and 10). The reconnection rate is then enhanced thanks to the Hall term, which gives rise to the whistler dynamics and decouples the electron and ion motion (e.g., see Ref. 8).

At lower β, the physics of fast reconnection is still under investigation. Theoretical (e.g., see Ref. 9) and experimental[6] results provide strong evidence that fast reconnection still occurs in lower β plasmas, but the reconnection rate is reduced. However, the scaling of the reconnection rate with the plasma β and the mass ratio has not been clarified completely. Theoretical studies[11–13] have proposed kinetic Alfvén wave (KAW) dynamics as the mechanism that enables fast reconnection in lower β plasmas, but the signature for this mechanism has been observed only in fluid simulations.[14] Recently, for $\beta \approx 1$ plasmas, evidence has been presented that the off-diagonal terms of the electron pressure tensor break the frozen-in condition[15,16] but it is not known what happens in lower β plasmas. In low β plasmas, drift motions are responsible for a typical asymmetry in the ion and electron motion in the reconnection plane,[9,16] but how the velocities depend on the mass ratio and plasma β has not been examined in detail.

The aim of the present paper is to study magnetic reconnection in plasmas with different β values, using kinetic simulation to study reconnection at low plasma β with mass ratios up to the physical value. The reconnection process is simulated using two particle-in-cell (PIC) codes, which model both kinetic ions and electrons. One is CELESTE3D, an implicit PIC code,[17–19] which is particularly suitable for large scale simulations with high mass ratios, and the other NPIC, a two-dimensional massively parallel explicit code,[20,21] which is much more expensive to run but which resolves all scales. The initial condition is a perturbed Harris sheet equilibrium and the system is permitted to evolve freely. The plasma β is changed by varying the intensity of the initial guide field, ranging from $\beta \gg 1$ (no guide field case), to $\beta < 1$ (strong guide field).

It should be remarked that other physical systems have been considered in the literature in order to study reconnection in low β plasmas.[14,22–24] Nishimura *et al.*[22] consider a

[a)]Electronic mail: paolo.ricci@polito.it
[b)]Electronic mail: jub@lanl.gov
[c)]Electronic mail: daughton@lanl.gov
[d)]Electronic mail: lapenta@lanl.gov

sheet pinch equilibrium[23] and analyze the growth of tearing and Buneman instabilities. Drake *et al.*[24] simulate a thin double current layer in three dimensions, in which the total magnetic field B and density are constant. The simulations show the development of turbulence that collapses in structures where the electron density is depleted. Rogers *et al.*[14] consider fluid simulations of wider current layers and point out that both the total β and the β based on the reconnecting field $[\beta_x = 8\pi n_0(T_i+T_e)/B_{x0}^2$, where B_{x0} is the asymptotic reconnecting field$]$ play an important role in determining the structure of the out-of-plane field and pressure profiles. (In our simulations, the total β is varied, while β_x is held fixed.) The conclusions described in the literature above do not apply directly to our results because they are based on different equilibria.

Our simulations yield several new results. First, we determine the scaling of the reconnection rate with large guide fields and high mass ratios. Second, we identify the mechanism by which the frozen-in condition is broken in the presence of a strong guide field, a crucial problem in the physics of reconnection. Third, we analyze the influence of the guide field on the in-plane and out-of-plane ion and electron velocities. Fourth and final, we demonstrate through our fully kinetic simulations with a strong guide field the typical electron density pattern related to the KAW dynamics previously predicted by theoretical studies[12] and shown by fluid simulations.[14]

The paper is organized as follows. Section II describes the physical problem and the numerical approach. Section III presents the results of the simulations, studies the mechanism for reconnection, analyzes the motion of ions and electrons, and examines the scaling of the reconnection rate with the mass ratio and the guide field.

II. THE SIMULATIONS

A Harris current sheet is considered in the (x,z) plane,[25] with an initial magnetic field given by

$$\mathbf{B}_0(z) = B_0 \tanh(z/\lambda)\mathbf{e}_x + B_{y0}\mathbf{e}_y . \tag{1}$$

The Harris configuration is an exact Vlasov equilibrium with ion and electron distributions given by

$$f_{0s} = \frac{n_0 \operatorname{sech}^2(z/\lambda)}{\pi^{3/2} v_{th,s}^3} \exp\left[-\frac{v_x^2 + (v_y - V_{s0})^2 + v_z^2}{v_{th,s}^2} \right] + \frac{n_b}{\pi^{3/2} v_{th,s}^3} \exp\left(-\frac{v^2}{v_{th,s}^2} \right), \tag{2}$$

where V_{s0} is the drift velocity and $v_{th,s} = \sqrt{2T_s/m_s}$ is the thermal velocity.

The current carried by species s is given by

$$J_s = q_s n_0 V_{s0} \operatorname{sech}^2(z/\lambda) \tag{3}$$

and the plasma density given by

$$n_0(z) = n_0 \operatorname{sech}^2(z/\lambda) + n_b . \tag{4}$$

The GEM physical parameters are used.[8] The temperature ratio is $T_i/T_e = 5$, the current sheet thickness is $\lambda = 0.5 d_i$, the background density is $n_b = 0.2 n_0$, the ion drift velocity in the y direction is $V_{i0} = 1.67 V_A$, where V_A is the Alfvén velocity defined with the density n_0 and the field B_0, and $V_{e0}/V_{i0} = -T_e/T_i$. The equilibrium current is mostly carried by ions because $V_{i0} = -5V_{e0}$. The ion inertial length, $d_i = c/\omega_{pi}$, is defined using the density n_0.

TABLE I. Decrease of the error in the energy conservation, $\Delta E(t) = [E_{\mathrm{tot}}(t) - E_{\mathrm{tot}}(0)]/E_{\mathrm{tot}}(0)$, at time $t\omega_{ci} = 40$ when the time step is reduced. We consider a set of CELESTE3D simulations with $m_i/m_e = 25$, $B_y/B_{y0} = 5$, 64×64 grid points, and 200 particles per cell. The NPIC energy conservation is shown for comparison.

$\Delta t\omega_{pi}$	ΔE
0.30	0.096
0.15	0.034
0.08	0.009
0.03	-2.2×10^{-4}
Explicit (0.014)	5.6×10^{-4}

The standard GEM challenge is modified by introducing an initially uniform guide field $B_y = B_{y0}$ $(B_{y0} = 0, B_0, 5B_0)$, which eliminates the line of null magnetic field for $B_{y0} \neq 0$. Different mass ratios are used, $m_i/m_e = 25$ (standard GEM mass ratio), $m_i/m_e = 180$, and the physical mass ratio for hydrogen $m_i/m_e = 1836$. Following Ref. 8, the Harris equilibrium is modified by introducing an initial flux perturbation in the form

$$A_y = -A_{y0}\cos(2\pi x/L_x)\cos(\pi z/L_z), \tag{5}$$

with $A_{y0} = 0.1 B_0 c/\omega_{pi}$. The perturbation introduces in the Harris current sheet a seed magnetic island with X point at $x=0$ and $z=0$. This magnetic island develops and grows during reconnection.

The boundary conditions for the particles and fields are periodic in the x direction. Conducting boundary conditions are imposed for the fields at the z boundaries while reflecting boundary conditions are used for the particles.

The simulations shown in the present paper are performed using two PIC codes, CELESTE3D, an implicit PIC code, and NPIC, an explicit simulation code. The implicit PIC method, and particularly the code CELESTE3D, has been applied to many problems in plasma physics in one dimension,[26] in two dimensions,[10,18,27–30] and three dimensions.[31–33] NPIC has been used to study the dynamics of thin current layers.[34,35]

CELESTE3D solves the full set of Maxwell–Vlasov equations using the implicit moment method.[17–19] The implicit moment method allows simulations on ion length and time scales, while retaining the kinetic effects on these scales for both electrons and ions. Both Maxwell's equations and the particle equations of motion are discretized implicitly in time. With large time steps, the discretized equations model a quasineutral plasma, in which random fluctuations in the electrostatic field are much reduced compared with an explicit solution with the same number of particles, and smooth solutions are obtained with a relatively small number of particles per cell.

The explicit plasma simulation code NPIC is based on a well-known explicit electromagnetic algorithm.[20,21] Maxwell's equations are advanced in time using either a simple explicit algorithm[21] or a semi-implicit method that permits

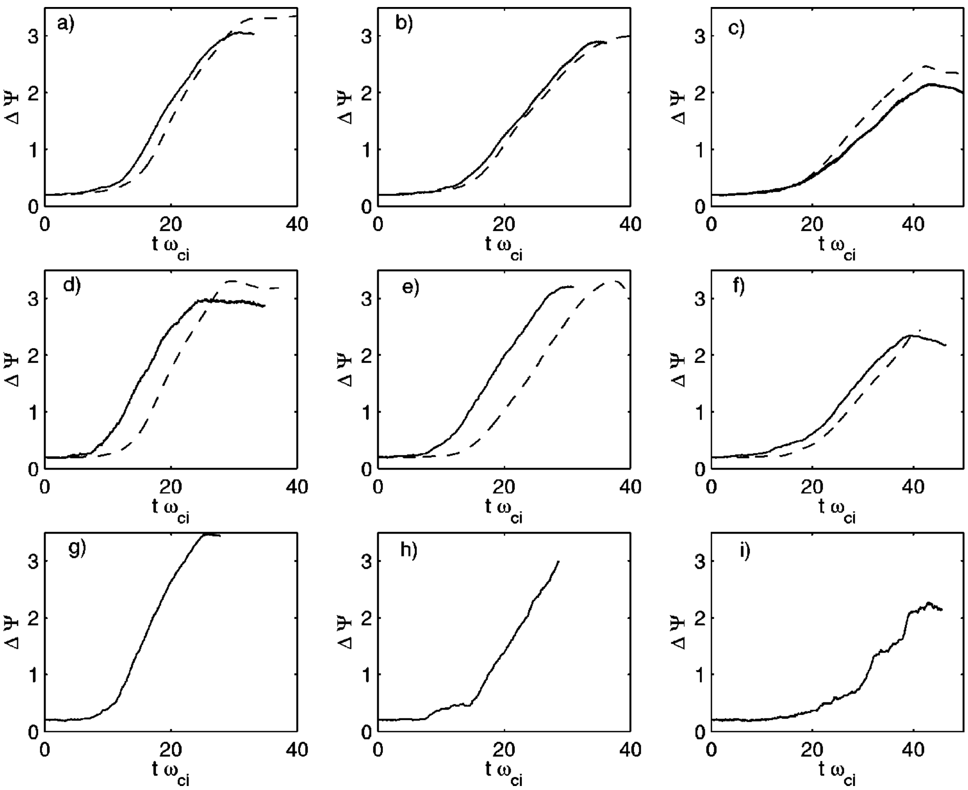

FIG. 1. The reconnected flux is plotted for $m_i/m_e=25$ and $B_{y0}=0$ (a), $m_i/m_e=25$ and $B_{y0}=B_0$ (b), $m_i/m_e=25$ and $B_{y0}=5B_0$ (c), $m_i/m_e=180$ and $B_{y0}=0$ (d), $m_i/m_e=180$ and $B_{y0}=B_0$ (e), $m_i/m_e=180$ and $B_{y0}=5B_0$ (f), $m_i/m_e=1836$ and $B_{y0}=0$ (g), $m_i/m_e=1836$ and $B_{y0}=B_0$ (h), and $m_i/m_e=1836$ and $B_{y0}=5B_0$ (i). The reconnected flux is normalized to B_0c/ω_{pi}. The results from CELESTE3D (solid line) and NPIC (dashed) are plotted.

the time step to exceed the Courant limit.[20] This corresponds to an implicit treatment of light waves, while the rest of the algorithm remains explicit and the electron plasma frequency and cyclotron motion are fully resolved. In this manuscript, all simulations at low mass ratio $m_i/m_e=25$ were performed with the simple explicit version of the field solver, while two of the simulations at higher mass ratio ($m_i/m_e=180$, $B_{y0}=0$, B_0) were performed with the semi-implicit version of the field solver with a time step approximately three times larger than the Courant limit. For the strong guide field high mass ratio case ($m_i/m_e=180$, $B_{y0}=5B_0$), the simple explicit field solver was employed since the time constraint imposed by the guide field on the particle mover is more limiting. Extensive comparisons between the two versions of the field solver have revealed no significant differences. NPIC is run on a parallel computer using domain decomposition with calls to the Message Passing Interface (MPI) library.

The explicit simulation is much more expensive because it must observe the time step limit, $\Delta t<2/\omega_{pe}$, and the mesh spacing required to avoid the finite grid instability, $\Delta x \leqslant 2\lambda_{De}$, with ω_{pe} and λ_{De} denoting the electron plasma frequency and Debye length. The implicit simulations must respect an accuracy condition, $v_{th,e}\Delta t<\Delta x$, whose principal effect is to determine how well energy is conserved (see Table I). In general, the accuracy condition permits much larger Δx and Δt than possible with explicit methods.

Explicit PIC simulations with higher mass ratios can be very expensive. The cost of an explicit simulation on ion time and space scales varies with the ion to electron mass ratio as $(m_i/m_e)^{(d+2)/2}$, where d is the number of spatial dimensions.[36] For example, in two dimensions, a simulation of the GEM challenge with $m_i/m_e=1836$ is more than 5000 times as expensive as one with $m_i/m_e=25$ if the explicit method is used. An implicit simulation, which scales as $(m_i/m_e)^{1/2}$, is much less expensive. (The time step can be kept constant with respect to the ion plasma frequency and the ratio ω_{ci}/ω_{pi} is scaled as $(m_i/m_e)^{1/2}$, in order to maintain the ratios ρ_i/L and $v_{th,e}/c$ constant.[10]) However, the explicit PIC method resolves all relevant scales within the plasma, and with a massively parallel computer, now even high mass ratio simulations are becoming feasible in two dimensions. The explicit simulations reported here stretch the limit of the current computational resources; 128 processors on the Los Alamos Q-machine were used. The implicit simulations, by comparison, are run on a commodity PC with a single Pentium IV processor.

The simulation parameters for CELESTE3D, with $m_i/m_e=25$, are a $N_x\times N_z=64\times 64$ grid, with time step $\omega_{pi}\Delta t=0.3$, and 25 particles per species per cell, for a total of 2×10^5 computational particles. For high mass ratios, the simulations are performed by CELESTE3D with the same simulation parameters, except for the $m_i/m_e=1836$ case where the time step is reduced to $\omega_{pi}\Delta t=0.1$.

The simulation parameters for NPIC, with $m_i/m_e=25$, are a $N_x\times N_z=1024\times 512$ grid, 104×10^6 computational particles and a time step corresponding to $\omega_{pi}\Delta t=0.029$ for $B_{y0}=0$, B_0, and $\omega_{pi}\Delta t=0.014$ at $B_{y0}=5B_0$. For the high mass ratio cases $m_i/m_e=180$, the simulation parameters are $N_x\times N_z=2560\times 1280$, 1×10^9 particles, and a time step $\omega_{pi}\Delta t=0.019$ for $B_{y0}=0$, B_0, and $\omega_{pi}\Delta t=0.0064$ at $B_{y0}=5B_0$. For the case $B_{y0}=5B_0$ and $m_i/m_e=25$, a more detailed explicit simulation with grid $N_x\times N_z=3072\times 1536$ has been performed, with time step $\omega_{pi}\Delta t=0.0065$, and with 1

TABLE II. Averaged reconnection rates, normalized to B_0V_A/c, as a function of the guide field and the mass ratio from CELESTE3D.

	$m_i/m_e=25$	$m_i/m_e=180$	$m_i/m_e=1836$
$B_{y0}/B_0=0$	0.179	0.190	0.206
$B_{y0}/B_0=1$	0.141	0.164	0.182
$B_{y0}/B_0=5$	0.086	0.099	0.113

TABLE III. Averaged reconnection rates, normalized to B_0V_A/c, as a function of the guide field and the mass ratio from NPIC.

	$m_i/m_e=25$	$m_i/m_e=180$
$B_{y0}/B_0=0$	0.176	0.199
$B_{y0}/B_0=1$	0.144	0.163
$B_{y0}/B_0=5$	0.091	0.106

$\times 10^9$ particles. In comparison to the simulations with grid $N_x\times N_z=1024\times 512$, the latter simulation does resolve the electron gyroradius, with grid spacing $\Delta x=\Delta z=0.016L$ and $\rho_e=0.032L$.

In general, as is discussed below the results from the two codes agree for the mass ratios $m_i/m_e=25,180$. CELESTE3D is also used to simulate the physical mass ratio $m_i/m_e=1836$. No comparison with NPIC is possible for this case, since only CELESTE3D can do this problem.

In conclusion, the strength of our approach is that it is based on two independent codes with complementary capabilities. It should be remarked that this degree of verification is rarely observed in the literature.

III. SIMULATION RESULTS

A set of simulations is performed, using different mass ratios ($m_i/m_e=25$, $m_i/m_e=180$, and $m_i/m_e=1836$) and different guide fields: the standard GEM challenge with $B_{y0}=0$, $B_{y0}=B_0$, and $B_{y0}=5B_0$, corresponding to $\beta=\infty$, $\beta=1.2$, and $\beta=0.048$, in the center of the current sheet $[\beta=8\pi(n_0+n_b)(T_i+T_e)/B_{y0}^2]$.

In all cases, the typical evolution of the magnetic flux and the out-of-plane current is similar to the picture of magnetic reconnection in the absence of a guide field provided by the GEM challenge project (e.g., in Ref. 18). In particular, in the presence of a guide field reconnection still occurs but it requires a longer time and saturates at a lower level. The current is considerably more filamentary and peaks of negative current appear which are not present in the standard GEM challenge with no guide field.

In Fig. 1, the reconnection flux as a function of time for both NPIC and CELESTE3D simulations are shown. The reconnected flux is measured as the flux difference $\Delta\Psi$ between the X and the O points. Simulations are performed with $m_i/m_e=25,180,1836$ with the implicit PIC code CELESTE3D and with $m_i/m_e=25,180$ for the explicit PIC code NPIC. All the simulations show a similar evolution. After slow initial growth, which lasts until $t\omega_{ci}\approx 10$ (or longer, for higher guide fields), reconnection enters a fast phase that persists until the saturation level is reached. During the fast reconnection phase, both NPIC and CELESTE3D (when simulations with enhanced spatial resolution are performed) show multiple small scale islands, which merge at later time into a single island. The saturation level decreases with the guide field, because the out-of-plane magnetic field influences the plasma motion reducing its compressibility.

The reconnection rates that best fit the fast reconnection phase are listed in Table II for CELESTE3D and in Table III for NPIC. In general, the reconnection rate decreases as the guide field increases for all values of the mass ratio, as the fast reconnection mechanism becomes less efficient in low-β plasmas. Both CELESTE3D and NPIC show that the reconnection rate increases weakly with the mass ratio for all the guide fields considered.

For the reconnected flux, the results of the explicit and implicit simulations agree remarkably well for both mass ratios and all the guide fields. As Tables II and III show, the two codes give reconnection rates within 5% of each other. Also, the saturation levels are similar in the two codes. It should be remarked that, in some cases, the fast reconnection phase starts later in explicit simulations. The later start is due to the reduced initial noise in the explicit simulation because of a much larger number of particles.

A study of sensitivity of the explicit simulation to the simulation parameters is shown in Fig. 2. The reconnected flux is plotted for $m_i/m_e=25$ and $B_{y0}=5$ as a function of time, for two NPIC simulations: the standard resolution simulation ($N_x\times N_z=1024\times 512$ grid, $\omega_{pi}\Delta t=0.014$, and 2×10^5 particles) and the higher resolution simulation that does resolve the electron gyromotion ($N_x\times N_z=3072\times 1536$ grid, $\omega_{pi}\Delta t=0.0065$, and 1×10^9 particles). The slope of the two is very similar in both runs. The only noticeable difference is a later start of the fast reconnection phase for the higher resolution case, confirming that an increased number of particles (i.e., a reduced initial noise) postpones the fast reconnection phase.

The energy associated with the different components of the magnetic field, and the electron and ion kinetic energy are plotted in Fig. 3. The reconnection process causes a decrease of the total magnetic energy, because the x component of the magnetic field is destroyed by the reconnection pro-

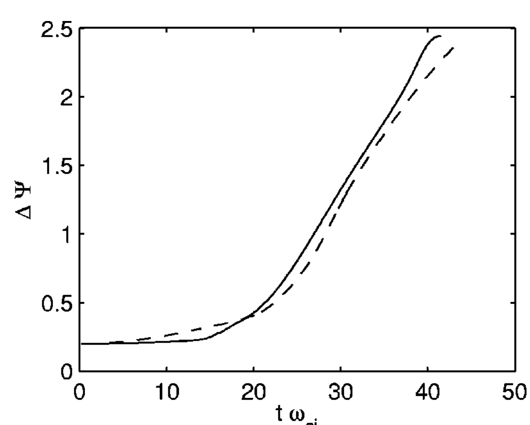

FIG. 2. The reconnected flux is plotted for $m_i/m_e=25$ and $B_{y0}=5$ as a function of time, for two NPIC simulations: $N_x\times N_z=1024\times 512$ grid, $\omega_{pi}\Delta t=0.014$, and 2×10^5 particles (solid); $N_x\times N_z=3072\times 1536$ grid, $\omega_{pi}\Delta t=0.0065$, and 1×10^9 particles (dashed).

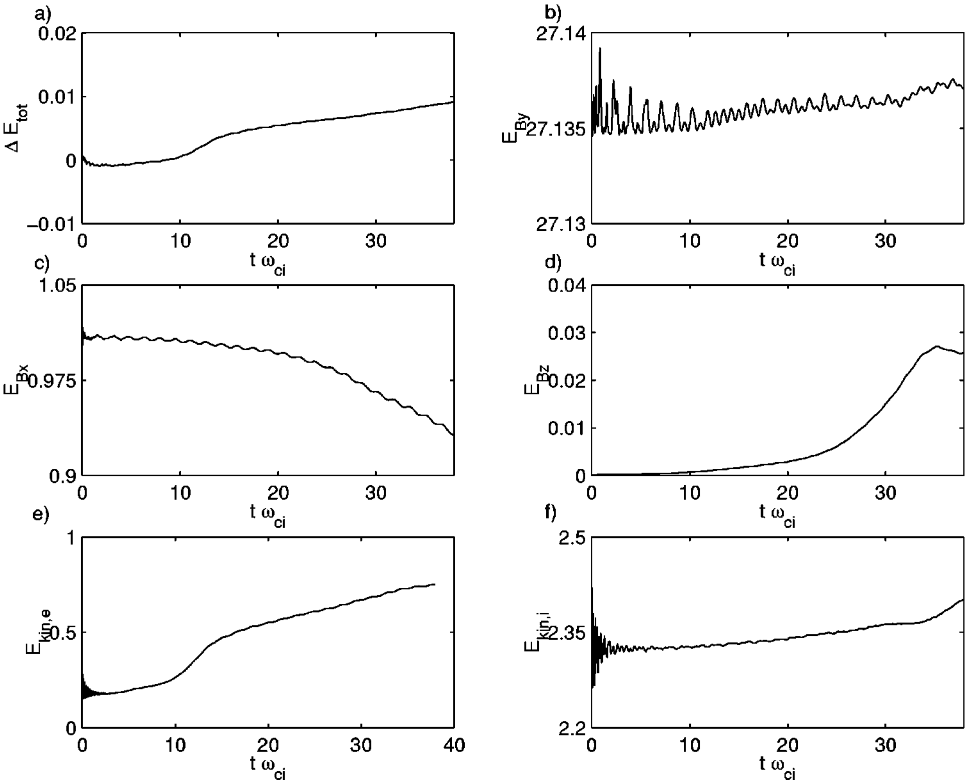

FIG. 3. Plotted are the relative variation of the total energy of the plasma, $[E_{\mathrm{tot}}(t)-E_{\mathrm{tot}}(0)]/E_{\mathrm{tot}}(0)$ (a); the energy of the y component of the magnetic field, E_{By} (b); the energy of the x component of the magnetic field, E_{Bx} (c); the energy of the z component of the magnetic field, E_{Bz} (d); the electron kinetic energy, $E_{kin,e}$ (e), and the ion kinetic energy, $E_{kin,i}$ (f) for the CELESTE3D simulation with $m_i/m_e=25$, $\omega_{pi}\Delta t=0.08$, and $B_{y0}=5B_0$. The energies are normalized to $E_{Bx}(0)$.

cess. In particular our results show that, while the energy related to the y component of the magnetic field is almost constant (it slightly increases in the $B_y=0$, B_0 case), the B_x field energy decreases, and the energy of the z component of the magnetic field, which is created during the reconnection process, grows. The lost magnetic energy is transferred to the ions and electrons in form of kinetic energy.

In the following section, the mechanism which leads to the breakup of the frozen-in condition for electrons is analyzed, and the general motion of ions and electrons depending on the guide field is studied. Finally, the mechanism of fast reconnection is pointed out, when the whistler dynamics are suppressed by the presence of the guide field.

A. Violation of the frozen-in condition

The frozen-in condition is a characteristic property of ideal magnetohydrodynamics (MHD) plasmas, which forces plasma and magnetic fields to move together. As long as the frozen-in condition is satisfied, the magnetic field topology cannot change and reconnection cannot take place.[1] Reconnection cannot occur unless some mechanism breaks the frozen-in condition. Once the frozen-in condition is broken, the plasma particles can move relative to the magnetic field, and the magnetic field lines can reconnect and change their topology.

Fundamentally, the frozen-in condition follows from the assumption of ideal plasmas, where Ohm's law reduces to ideal terms only. However, in collisionless plasmas the complete Ohm's law includes a number of terms neglected in the ideal MHD limit that can be significant and can potentially break the frozen-in condition. The complete Ohm's law states that the reconnection electric field, which is proportional to the reconnection rate, can be expressed as (e.g., see Ref. 1)

$$E_{y,rec}=-\frac{1}{c}(v_{ze}B_x-v_{xe}B_z)-\frac{1}{en_e}\left(\frac{\partial P_{xye}}{\partial x}+\frac{\partial P_{yze}}{\partial z}\right)-\frac{m_e}{e}\left(\frac{\partial v_{ye}}{\partial t}+v_{xe}\frac{\partial v_{ye}}{\partial x}+v_{ze}\frac{\partial v_{ye}}{\partial z}\right), \tag{6}$$

where the resistive term is not included, since it is rigorously zero in collisionless plasmas.

At the X point, the magnetic field components B_x and B_z vanish and the only contributions to the reconnection electric field are given by gradients of the off-diagonal terms of the electron pressure and electron inertial effects. A considerable debate has taken place in the literature among supporters of one or the other of the two mechanisms.

In the zero guide field case, the general consensus is that the off-diagonal terms of the pressure tensor are the main players, while the electron inertia is negligible. Kutnetsova *et al.*[37] show that the electrons become demagnetized near the X point, at distances comparable to the electron meandering lengths,

$$d_{xe}=\left[\frac{c^2m_eT_e}{e^2(\partial B_z/\partial x)^2}\right]^{1/4},\quad d_{ze}=\left[\frac{c^2m_eT_e}{e^2(\partial B_x/\partial z)^2}\right]^{1/4}, \tag{7}$$

and execute a bounce motion which results in the presence of off-diagonal terms of the electron pressure tensor. In this case, the off-diagonal terms of the electron pressure are most important in breaking the frozen-in condition.[9,10]

In the presence of a guide field, no established result has yet been agreed upon. Evidence has been given that the elec-

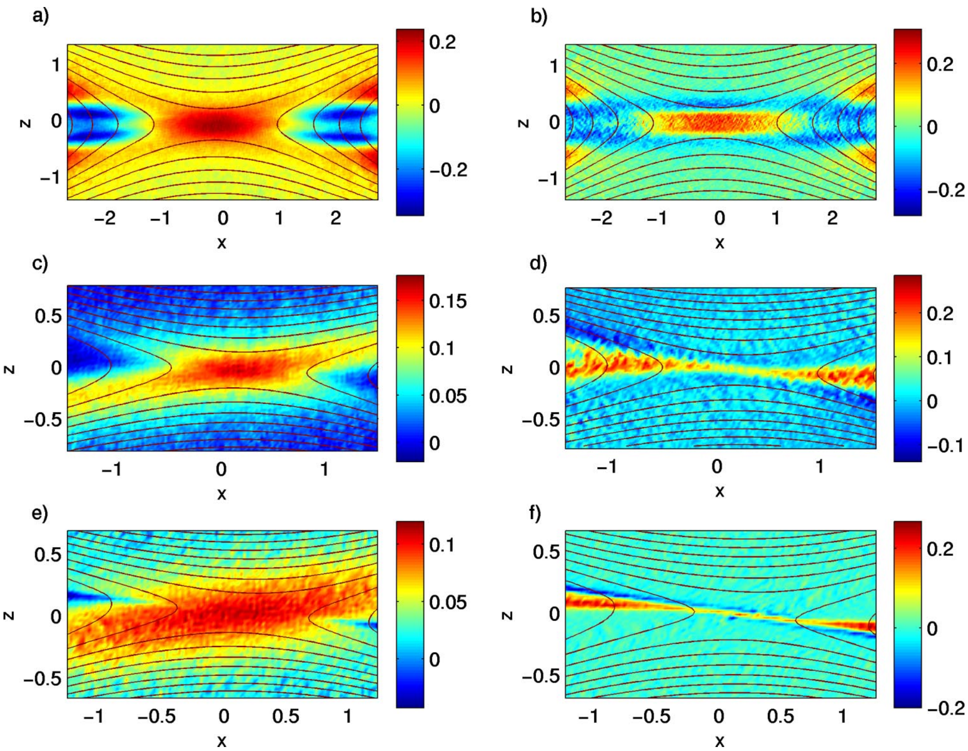

FIG. 4. (Color online). For $m_i/m_e=25$, results from NPIC are shown for the nonideal part of the reconnection electric field, $E_y+(v_{ze}B_x-v_{xe}B_z)/c$, (a,c,e) and electron pressure contribution to the electric field (b,d,f), $-1/en_e(\partial P_{xye}/\partial y+\partial P_{zye}/\partial z)$. Both plots are color coded, and normalized to B_0V_A/c. The magnetic field lines are plotted in all frames and the guide fields are $B_{y0}=0$ (a,b), $B_{y0}=B_0$ (c,d), and $B_{y0}=5B_0$ (e,f). E_y is normalized to B_0V_A/c. The results are plotted at a time when $\Delta\Psi=1$. The data are averaged over 100 time slices separated by 10 time intervals with $\Delta t\omega_{pi}=0.014$.

tron pressure is still the mechanism that allows reconnection in presence of a weak guide field ($B_{y0}=0.3B_0$, $B_{y0}=0.8B_0$).[15,16] In the present work we consider larger guide fields and investigate what mechanism breaks the frozen-in condition.

Figures 4 and 5 show the nonideal part of out-of-plane electric field [i.e., $E_y+(v_{ze}B_x-v_{xe}B_z)/c$, which is the difference between the electric field E_y and the ideal terms $\mathbf{v}_e\times\mathbf{B}/c$], and the contribution of the electron pressure terms close to the X point during the reconnection process. Simulations performed by NPIC (Fig. 4) and CELESTE3D (Fig. 5) with the guide fields $B_{y0}=0$, $B_{y0}=B_0$, and $B_{y0}=5B_0$ are considered for a mass ratio $m_i/m_e=25$.

In the $B_{y0}=0$ case, we confirm the previous findings predicting that the electron pressure tensor is the dominant contribution at the X point (e.g., see Refs. 9 and 10) on a scale length of the order of the electron meandering length.[10]

For $B_{y0}=B_0$ and $B_{y0}=5B_0$, the symmetry of the

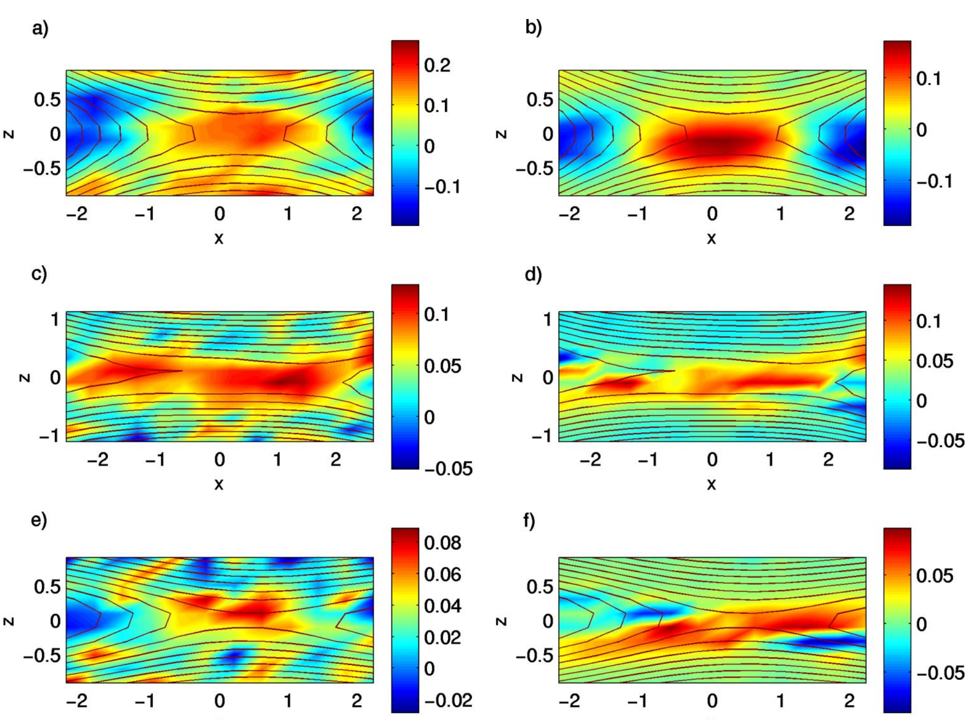

FIG. 5. (Color online). The corresponding results to Fig. 4 from CELESTE3D are shown. The data are averaged over a moving window of 100 time steps, with $\Delta t\omega_{pi}=0.03$.

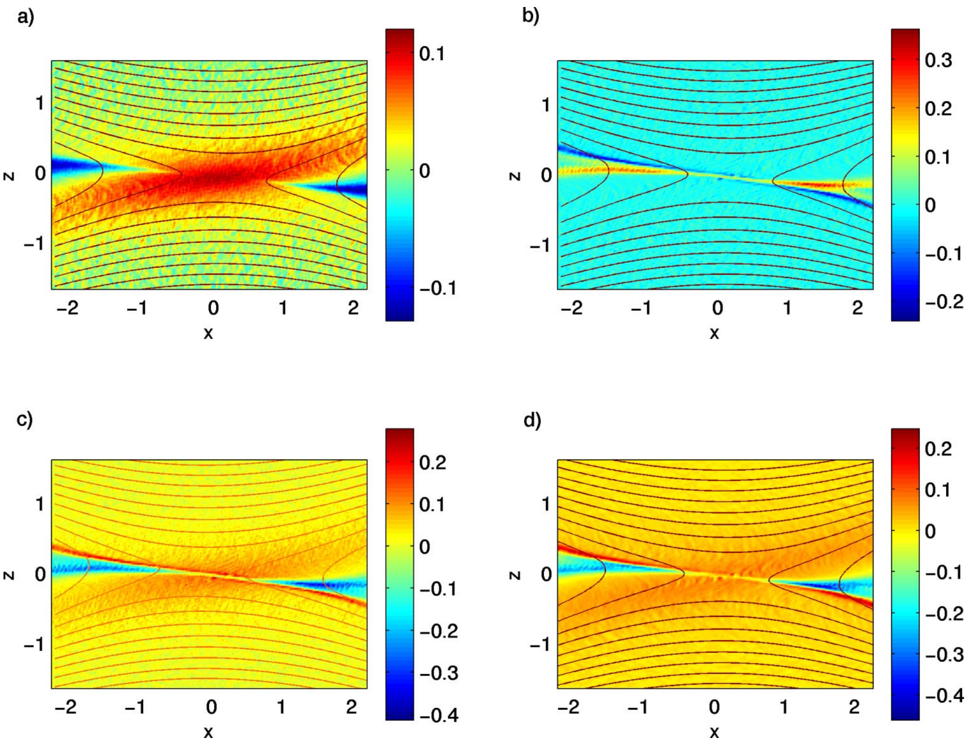

FIG. 6. (Color online). Contributions to the nonideal reconnection electric field $E_y+(v_{ze}B_x-v_{xe}B_z)/c$ (normalized to B_0V_A/c) (a) given by electron pressure terms $(\partial P_{xye}/\partial y+\partial P_{zye}/\partial z)$ (b); $v_{xe}\partial v_{ye}/\partial x+v_{ze}\partial v_{ye}/\partial z$ (c) and by all the inertia terms, evaluated as the difference between the nonideal electric field and the pressure contribution. (d) We consider $m_i/m_e=25$, $B_{y0}=5B_0$. The results are plotted at a time when $\Delta\Psi=1$. These results are from NPIC, and represent average over 100 time slices separated each other by a time step $\Delta t\omega_{pi}=0.14$.

break-up region seen in the $B_{y0}=0$ case is lost and is replaced by a more complex nonsymmetric structure. Figures 4 and 5 show that the electron pressure is the dominant nonideal term with $B_{y0}=B_0$ and $B_{y0}=5B_0$.

It should be remarked that the out-of-plane electron velocity evaluated from both simulations shows that electron inertia alone cannot be responsible for the break-up mechanism. Figure 6, which shows results for the case $m_i/m_e=25$ and $B_{y0}=5B_0$ from NPIC, allows one to study the contributions to the nonideal electric field [plotted in Fig. 6(a)]. In Fig. 6(b) are shown the off-diagonal terms of the electron pressure tensor, in Fig. 6(c) the convective inertial terms, $v_{xe}\partial v_{ye}/\partial x+v_{ze}\partial v_{ye}/\partial z$, and in Fig. 6(d) the inertial term, computed as the difference between the nonideal electric field and the pressure contribution. As in the zero guide field case, the pressure terms dominate in the region closest to the X point, while the inertia terms are relevant at intermediate lengths. The contribution of the term $\partial v_{ye}/\partial t$ appears small because Figs. 6(c) and 6(d) are similar. The ideal terms give the main contribution far away from the reconnection region. According to these results, the importance of the pressure terms does not decrease in presence of a guide field. However, the spatial thickness of the region in which these terms dominate is of order ρ_e and thus decreases with increasing guide field.

If the off-diagonal terms of the pressure tensor are indeed responsible for breaking the frozen-in condition and allowing electrons to move relative to the magnetic field lines, thereby enabling reconnection to take place, what is the cause of the presence of off-diagonal terms of the pressure tensor in the first place?

To study the origin of off-diagonal terms of the pressure tensor, the simple approximations upon which most fluid models are based are no longer valid. More advanced fluid models incorporating the presence of off-diagonal terms for the pressure tensor have been recently designed to study the specific issue being considered here.[15] Based on the theoretical derivations, the off-diagonal components of the pressure are generated by gradients of the electron flow velocity in the y direction and by differences in the diagonal terms of the pressure tensor

$$P_{xye}=-\frac{P_{zze}}{\omega_{ce}}\frac{\partial v_{ye}}{\partial z}+\frac{B_x}{B_y}(P_{yye}-P_{zze}), \tag{8}$$

$$P_{yze}=-\frac{P_{xxe}}{\omega_{ce}}\frac{\partial v_{ye}}{\partial x}+\frac{B_z}{B_y}(P_{yye}-P_{xxe}), \tag{9}$$

where the heat flux has been ignored. It is assumed that $B_y\gg B_x$ and $B_y\gg B_z$, that the diagonal components of the pressure tensor are much larger than the off-diagonal components, and that $\tau\gg L/v_e$, where τ is a typical evolution scale, v_e is a typical electron velocity, and L is a typical scale length.

For the $B_{y0}=5B_0$ case, Fig. 7 compares the actual value of P_{xye} and P_{yze} obtained from the simulation, with the value computed from Eqs. (8) and (9), for the NPIC simulation. Once again, there is a good agreement between the simulation results and the theoretical predictions. The contribution to the off-diagonal terms in Eqs. (8) and (9) have been evaluated separately. It has been found that $P_{zze}/\omega_{ce}\partial v_{ye}/\partial z$ plays an important role in the evaluation of P_{xye}, while the contribution of $P_{xxe}/\omega_{ce}\partial v_{ye}/\partial x$ is not important to P_{yze} and thus $P_{yze}\approx B_z(P_{yye}-P_{xxe})/B_y$. CELESTE3D confirms these findings.

For $B_{y0}=0$ the results of the two codes are in very good agreement, although NPIC results are more refined because of the higher number of particles. For $B_{y0}=B_0$ and $B_{y0}=5B_0$, the results of the two codes need further discussion.

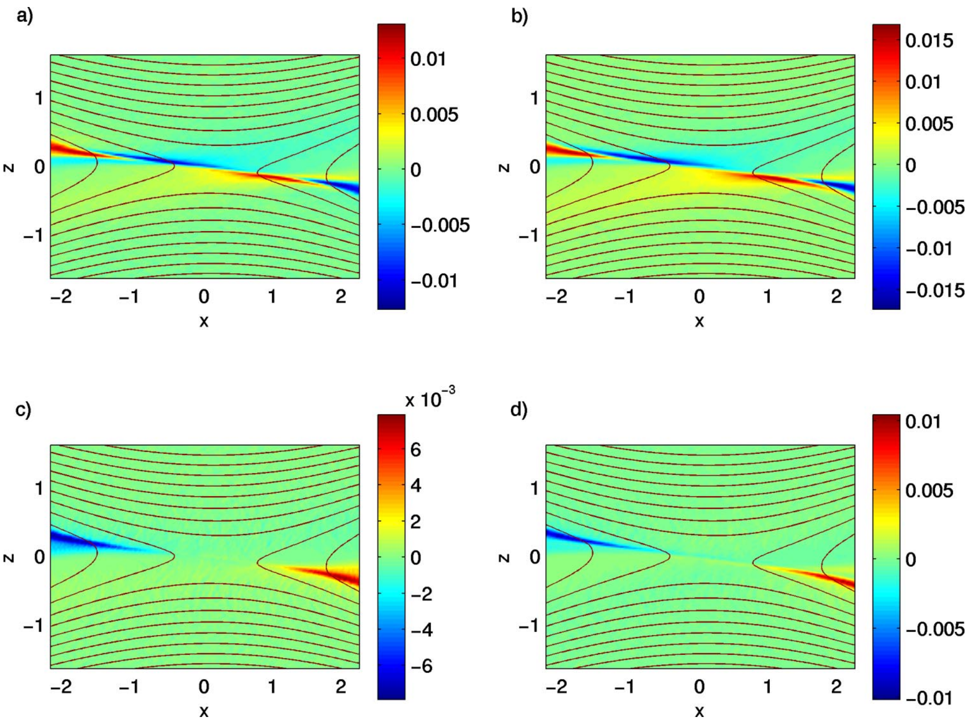

FIG. 7. (Color online). The actual off-diagonal terms of the electron pressure tensor from the NPIC simulation with $m_i/m_e=25$ and $B_{y0}=5B_0$ are plotted. Shown are P_{xye} (a), and P_{zye} (c), and their values computed from Eqs. (8) (b) and (9) (d). The results are plotted at a time when $\Delta\Psi=1$. The data are averaged over 100 time slices separated by a time step $\Delta t\omega_{pi}=0.14$.

Both NPIC and CELESTE3D do indicate that the contribution of the electron pressure tensor is responsible for the breakup of the frozen-in condition for all the guide fields. Moreover, the numerical value of the nonideal electric field at the X point and its pressure contribution, which is equal to the reconnection rate, are similar in the explicit and implicit simulations. However, only the higher spatial grid resolution of NPIC reveals that the characteristic thickness of the break-up region is of the order of a few ρ_e in presence of a guide field, while the implicit moment method spreads out the electron diffusion region from the electron gyroradius to a scale linked to the grid spacing.

As an aside, it should be pointed out that implicit simulations with $B_{y0}=5B_0$ that explore the electron break-up region are computationally very expensive, as they require the temporal resolution of the electron gyromotion.

B. Ion and electron motion

When $B_{y0}=0$, the ions and electrons $\mathbf{E}\times\mathbf{B}$ drift towards the X point along the z direction (see, e.g., Ref. 9). The ions become demagnetized at distances of the order of a few d_i, because of the Hall effect, are accelerated along the y direction by the reconnection electric field E_y and flow outwards in the x direction at the Alfvén speed, where they are diverted by the B_z magnetic field. The electrons follow a similar flow pattern, except that they are demagnetized at shorter distances, of the order of the electron meandering lengths [see Eq. (7)], and are expelled at super-Alfvénic velocities. The whole ion and electron motion is up-down and left-right symmetric.

The presence of a guide field rotates the $\mathbf{E}\times\mathbf{B}$ motion, causes ions and electrons to drift in directions not otherwise possible, and destroys the symmetry with respect to the $z=0$ axes. In Figs. 8 and 9, the ion and electron motion in the (x,z) plane is represented in the presence of a guide field.

In all cases, the ions are diverted when they approach the X point in an antisymmetric way with respect to the $x=0$

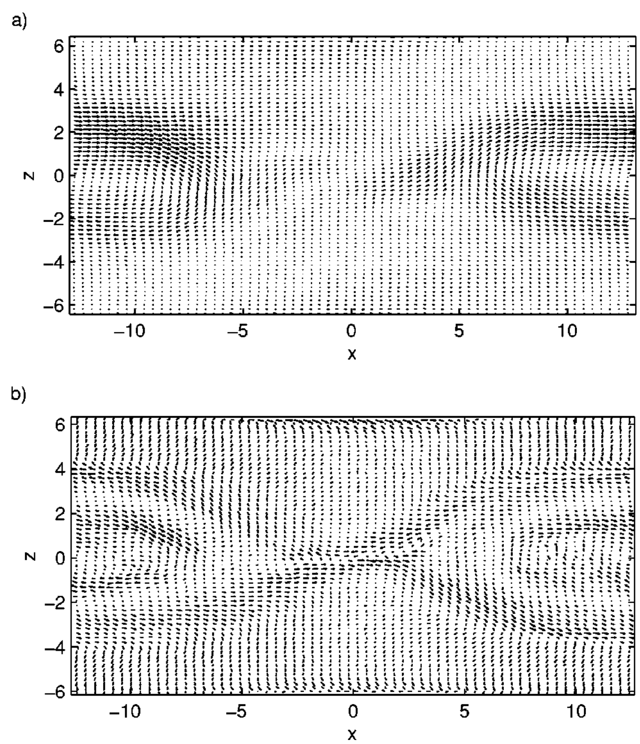

FIG. 8. Ion (a) and electron (b) motion in the (x,z) plane is shown for $m_i/m_e=25$ and $B_{y0}=B_0$. The results are plotted at a time when $\Delta\Psi=1$. These results are from CELESTE3D. The velocity vector magnitude is proportional to the arrow length, and the maximum magnitude is 0.70 V_A for ions and 4.06 V_A for electrons.

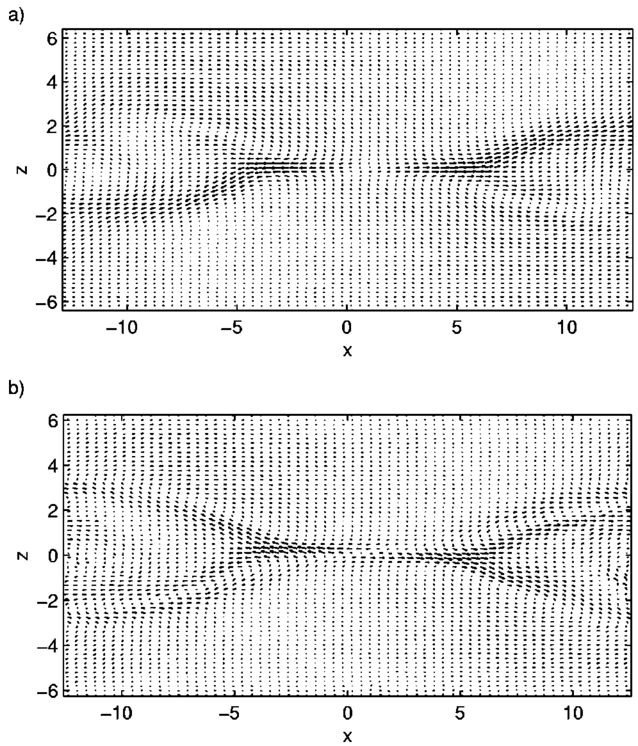

FIG. 9. Ion (a) and electron (b) motion in the (x,z) plane is shown for $m_i/m_e=25$ and $B_{y0}=5B_0$. The results are plotted at a time when $\Delta\Psi=1$. These results are from CELESTE3D. The velocity vector magnitude is proportional to the arrow length, and the maximum magnitude is 0.88 V_A for ions and 1.01 V_A for electrons.

line. Their outflow motion is primarily along x. The outflow region becomes smaller as the guide field increases. The electron dynamics are completely different and depend strongly on the guide field. In the $B_{y0}=B_0$ case (Fig. 8) electrons exhibit a strong flow along the separatrix. The motion is inward in the first and third quadrant, and outward in the second and fourth quadrants. Our simulation confirms the asymmetric motion of the electrons, which has been shown theoretically to have an important role in the reconnection process.[11–13] In the presence of a stronger guide field, $B_{y0}=5B_0$ (Fig. 9), the electrons flow with a similar pattern to the $B_{y0}=B_0$ case, but the in-plane motion is more localized.

The electron motion along the y direction (i.e., the out-of-plane direction of the guide field) is also affected by the guide field. This is shown in Fig. 10, where CELESTE3D and NPIC results are compared. When $B_{y0}=0$, the ions are accelerated by the reconnection electric field E_y at the X point along the y direction. However, the B_z field diverts the electrons, decreasing the y velocity, and forcing the outflow in the x direction. In the presence of a guide field, even far from the X point, the electrons maintain a significant velocity in the y direction, as they flow along the magnetic field. The electron motion is concentrated at the separatrix and the y velocity increases with the guide field.

Figure 11 shows the details of the electron distribution function. The histograms represent the distribution of the velocity v_x, v_y, and v_z in a region close to the X point, for different guide fields. In particular, the v_y distribution shows the presence of a drift that increases with the guide field. Moreover, in the case $B_{y0}=5B_0$, the presence of the background population is shown by a peak in the distribution near $v_{y0}=0$.

CELESTE3D results[38] reveal also a dependence of the out-of-plane velocity on the mass ratio, showing that lighter electrons reach higher velocities.

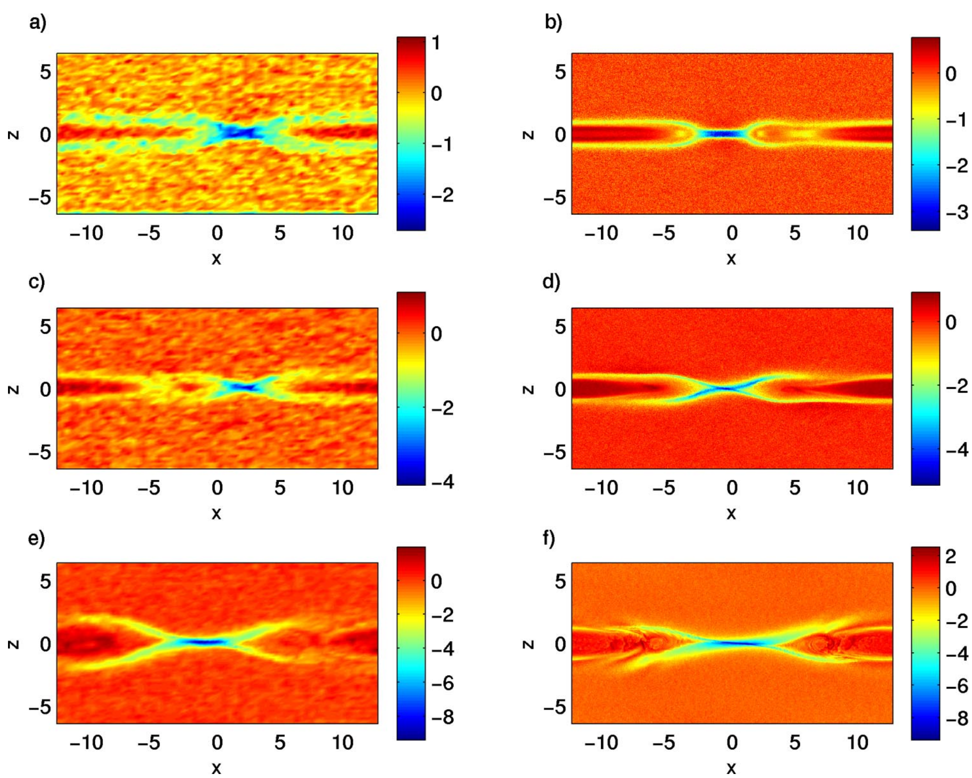

FIG. 10. (Color online). The electron velocity v_{ye} is shown at a time when $\Delta\Psi=1$, for $B_{y0}=0$ (a,b), $B_{y0}=B_0$ (c,d), $B_{y0}=5B_0$ (e,f), and mass ratio $m_i/m_e=25$. These results are from CELESTE3D (a,c,e) and NPIC (b,d,f). v_{ye} is normalized to V_A.

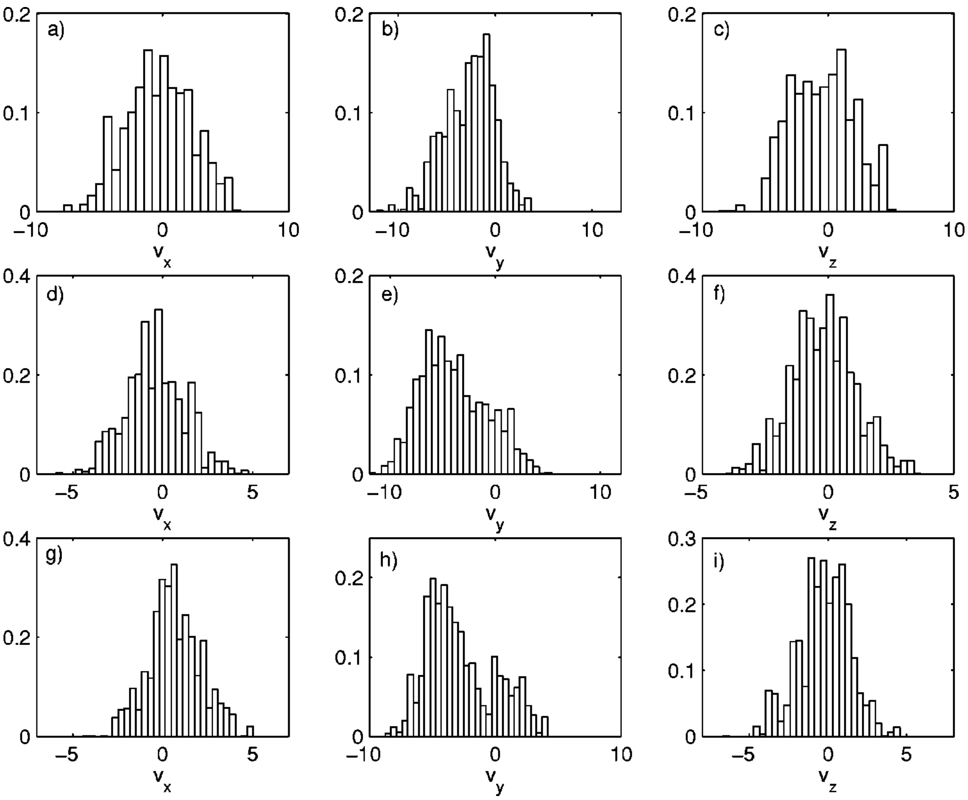

FIG. 11. Distribution of the electron velocities v_x, v_y, and v_z, from CELESTE3D simulations with $m_i/m_e=25$ and $B_{y0}=0$ (a–c), $B_{y0}=B_0$ (d–f), and $B_{y0}=5B_0$ (g–i). The results are plotted at a time when $\Delta\Psi=1$. The distributions consider the electrons located in the region of size $\Delta x=2c/\omega_{pi}$ and $\Delta z=0.5c/\omega_{pi}$ around the X point.

C. Fast reconnection mechanism

One of the main new development in the understanding of reconnection in the last few years has been the discovery of the importance of the presence of both an ion diffusion region and an electron diffusion region (see, e.g., Ref. 39). In the ion diffusion region, the electrons and the ions uncouple and while the electrons continue to be bound to the field lines by the frozen-in condition, the ions can flow freely. In the smaller electron diffusion region, the electrons become uncoupled as well and the reconnection process can change the topology of the field lines.

In Sec. III A, the mechanism active in the inner layer and responsible for uncoupling the electrons from the magnetic field has been studied and has been identified with the off-diagonal terms of the pressure tensor. In the present section, attention is focused on the outer layer, which is responsible for uncoupling the ions.

When $B_{y0}=0$, the Hall term in Ohm's law $\mathbf{J}\times\mathbf{B}$ decouples electron and ion motion and strongly enhances the reconnection rate. Because of the Hall effect, ion motion decouples from the electrons and the magnetic field at a distance of the order of d_i and the whistler dynamics are enabled. The whistler waves have a quadratic dispersion relation ($\omega\propto k^2$),[11] and a characteristic group speed that is inversely proportional to the length scale of the process. The dispersion is an essential component of Hall reconnection physics. As the scales are compressed within the ion layer, the outflow speed increases to balance the higher whistler wave speed, leading to a scale invariant reconnection rate. Thus, unlike the Sweet–Parker model where the outflow is limited by the Alfvén speed, the presence of the quadratic dispersion relation allows outflows from the inner electron layer at much higher speeds, thereby enabling fast reconnection. The mechanism is now well established and described in textbooks and articles, for example Refs. 1 and 40 give full descriptions. The typical signature of the Hall effect is the presence of a quadrupolar out-of-plane magnetic field,[41,42] which has also been observed by some satellite observations.[3]

At low β, the whistler dynamics are pushed to smaller scales,[11–13] because of magnetic field compression, $B_{y0}\boldsymbol{\nabla}\cdot\mathbf{v}$, which remains finite even if the motion is almost incompressible. Provided $\beta>m_e/m_i$ [i.e., $\rho_s>d_e$, $\rho_s^2=c^2m_i(T_e+T_i)/e^2B_{y0}^2$], parallel gradients of the electron pressure due to variations in electron density, $\nabla_\parallel n_e$, support a parallel electric field.[12] The dispersion corresponds to KAW, and is similar to the dispersion of the whistler wave ($\omega\propto k^2$). Thus fast reconnection is possible through the same mechanism described above.

The KAWs are characterized by a scale length ρ_s, which replaces d_i as the spatial scale of interest in presence of a guide field, and a quadrupolar density structure.[12] The electron density variation is due to an ion polarization drift, which causes the electron density gradient to reverse direction across the X point as the vertical magnetic field lines change polarity. Consequently, there is a quadrupolar pattern to the electron density and a parallel electric field that allows the ions to flow across B and reconnection to occur. This process happens on the scale length ρ_s. The electron density pattern in the presence of a guide field from a simulation is plotted in Fig. 12. The quadrupolar structure close to the reconnection region is as predicted, and has not been observed previously in kinetic simulations.

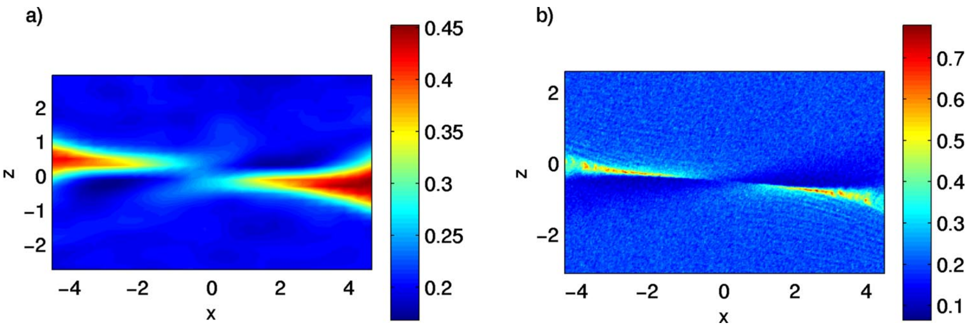

FIG. 12. (Color online). The electron density n_e is plotted for $m_i/m_e=25$ and $B_{y0}=5B_0$ at time $t\omega_{ci}=30$ in the reconnection region. The results are from CELESTE3D (a) and NPIC (b).

At still lower β ($\beta < m_e/m_i$), ions and electrons are tightly coupled, ions are forced to follow the electron dynamics, and fast reconnection is not possible. We have restricted our simulations to plasma βs for which fluid models predict fast reconnection. Our systematic kinetic study of fast reconnection as a function of the plasma β confirms the fluid results.

In Fig. 13, the out-of-plane magnetic field during the reconnection process is plotted for different mass ratios and different guide fields. In the zero guide field case, the out-of-plane magnetic field presents the typical quadrupolar symmetric structure due to the Hall effect. When a guide field is added to the initial Harris sheet equilibrium, the out-of-plane magnetic field is dramatically altered. The quadrupolar structure due to the Hall effect, is weakened and tilted at $B_{y0}=B_0$, and is unidentifiable for $B_{y0}=5B_0$. Even if the pattern of the magnetic field does not depend on the mass ratios, the maximum and minimum values are affected.

The width of the ion outflow region is shown in Fig. 14 for three different guide fields, by examining the x component of the ion velocity, v_{xi}. It is remarkable that for all guide fields, the ion outflow pattern is not influenced by the mass ratios. It follows that, at least for the range of guide fields studied, there is a mechanism that decouples the ion and electron dynamics (the electron dynamics depend on the mass ratio). Without a guide field, the outflow region is of the order of a few d_i. In the presence of the guide field $B_{y0}=B_0$, the outflow width decreases, and with a stronger guide field, $B_{y0}=5B_0$, the outflow region is narrower (Fig. 14). We note also that the scale length of interest, ρ_s, of this regime decreases when the guide field increases.

As Tables II and III show, the reconnection rate decreases as the guide field increases and the fast reconnection mechanism transitions occur from whistler dynamics to KAW dynamics. Experimental results confirm this trend[6] as well as previous numerical results.[9] A scaling law for the reconnection rate has been proposed with this same property.[43]

The reconnection rate shows only a weak dependence on the mass ratio. For $B_{y0}=0$, Shay and Drake[39] have demonstrated that the reconnection rate is insensitive to the physics that breaks the frozen-in condition. Consequently, the rate is

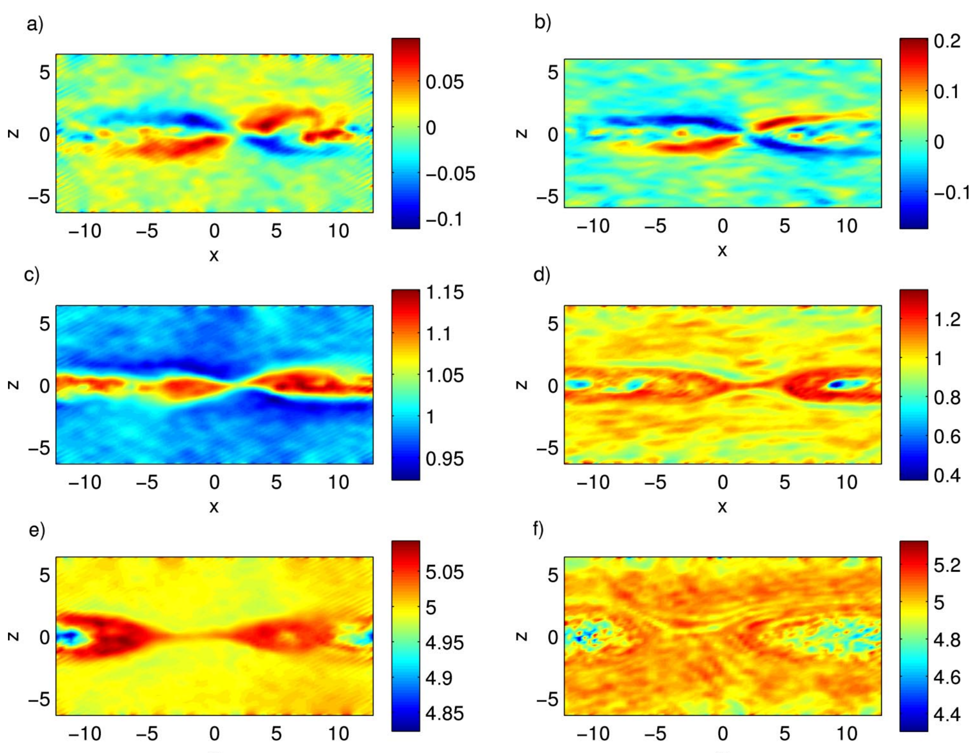

FIG. 13. (Color online). The magnetic field, B_y, is shown when $\Delta\Psi=1$, for $B_{y0}=0$ (a,b), $B_{y0}=B_0$ (c,d), $B_{y0}=5B_0$ (e,f), and mass ratio $m_i/m_e=25$ (a,c,e), $m_i/m_e=1836$ (b,d,f). These results are from CELESTE3D.

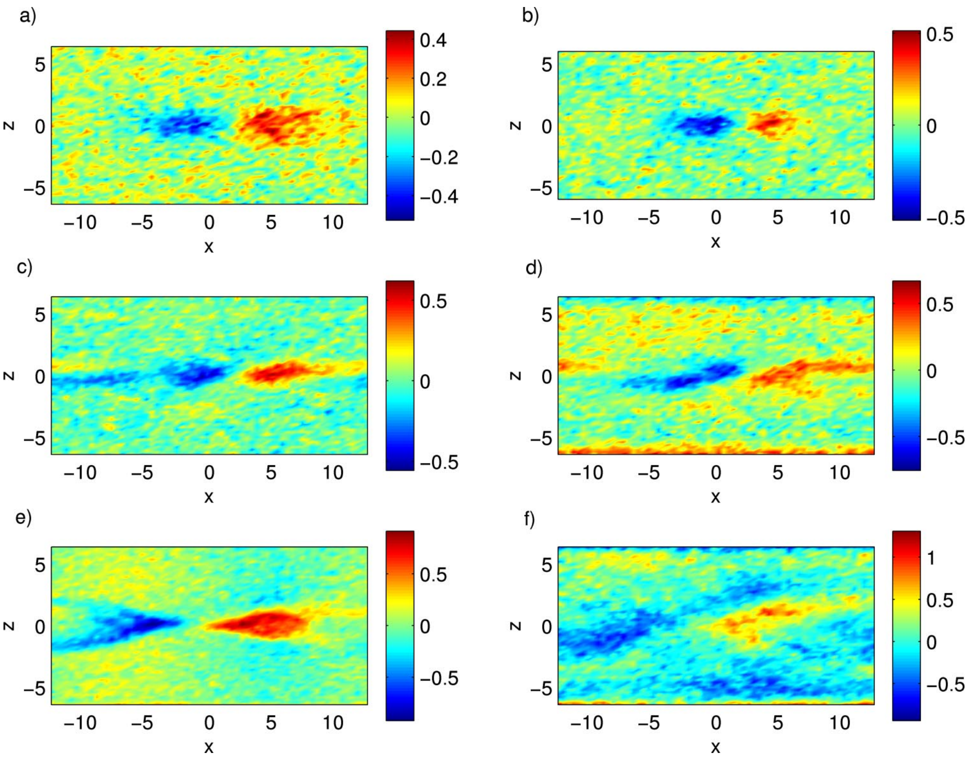

FIG. 14. (Color online). The ion velocity v_{xi} is plotted when $\Delta\Psi=1$, for $B_{y0}=0$ (a,b), $B_{y0}=B_0$ (c,d), $B_{y0}=5B_0$ (e,f), and mass ratio $m_i/m_e=25$ (a,c,e), $m_i/m_e=1836$ (b,d,f). These results are from CELESTE3D.

insensitive to the electron mass. This is confirmed by previous kinetic calculations extended to the physical mass ratio in Ref. 10.

IV. CONCLUSIONS

By performing kinetic simulations of Harris current sheets with different guide fields and different mass ratios, the physics of magnetic reconnection in plasmas characterized by different β values has been studied.

A main result of these simulations is the scaling of the reconnection rate with the guide field and the mass ratio, up to physical values. As in the case of high β plasmas, the mechanism which breaks the electron frozen-in condition is provided by the off-diagonal terms of the electron pressure tensor. The simulations extend the results to high guide fields, and demonstrate that the scale length of the diffusion region passes from the electron meandering length for $B_{y0}=0$ to the electron gyroradius as the guide field increases. The simulations indicate that the mechanism that allows fast reconnection changes with β. For high β, the typical quadrupolar structure of the out-of-plane magnetic field associated with whistler dynamics is present in the simulations. This mechanism decouples electrons and ions. At low β (high guide fields), KAW dynamics decouples electron and ions. The quadrupolar electron density pattern which characterizes KAW as predicted theoretically and by fluid models is observed in the simulations. The presence of a guide field causes additional components of the $\mathbf{E}\times\mathbf{B}$ drift, which modify the ion and electron motion causing asymmetric plasma flow.

The implicit and the explicit codes agree on the reconnection rate and the total reconnected flux, the structure of the out-of-plane magnetic field, and the electron velocity. Even though electron scales are not resolved by CELESTE3D, the electron gyrotropic pressure contributions are still clearly responsible for breaking the frozen-in condition, but they are distributed over a more extended spatial scale.

In closing, we note that an experimental setup has been built to study experimentally the dependence of reconnection on the guide field[5] and we plan to compare our simulation results with the experiments.

ACKNOWLEDGMENTS

The authors gratefully acknowledge useful discussions with J. Birn, P. Gary, R. Lovelace, M. Ottaviani, F. Porcelli, B. Rogers, M. Yamada, and L. Yin.

This research is supported by the LDRD program at the Los Alamos National Laboratory, by the United States Department of Energy, under Contract No. W-7405-ENG-36 and by NASA, under the "Sun Earth Connection Theory Program" and the "Geospace Sciences Program."

[1] D. Biskamp, *Magnetic Reconnection in Plasmas* (Cambridge University Press, Cambridge, England, 2000).
[2] E. R. Priest and T. Forbes, *Magnetic Reconnection: MHD Theory and Applications* (Cambridge University Press, Cambridge, England, 2000).
[3] M. Øieroset, T. D. Phan, M. Fujimoto, R. P. Lin, and R. P. Lepping, Nature (London) **412**, 414 (2001).
[4] A. Nishida, *Geomagnetic Diagnostics of the Magnetosphere* (Springer-Verlag, New York, 1978).
[5] I. Furno, T. Intrator, E. Torbert *et al.*, Rev. Sci. Instrum. **74**, 2324 (2003).
[6] M. Yamada, J. Geophys. Res. **104**, 14529 (1999).
[7] M. M. Romanova and R. V. E. Lovelace, Astron. Astrophys. **262**, 26 (1992).
[8] J. Birn, J. F. Drake, M. A. Shay *et al.*, J. Geophys. Res. **106**, 3715 (2001).
[9] P. L. Pritchett, J. Geophys. Res. **106**, 3783 (2001).
[10] P. Ricci, G. Lapenta, and J. U. Brackbill, Geophys. Res. Lett. **29**, 2008, 10.1029/2002GL015314 (2002).

[11]D. Biskamp, Phys. Plasmas **4**, 1964 (1997).
[12]R. G. Kleva, J. F. Drake, and F. L. Waelbroeck, Phys. Plasmas **2**, 23 (1995).
[13]B. N. Rogers, R. E. Denton, J. F. Drake, and M. A. Shay, Phys. Rev. Lett. **87**, 195004 (2001).
[14]B. N. Rogers, R. E. Denton, and J. F. Drake, J. Geophys. Res. **108**, 1111 (2003).
[15]M. Hesse, M. Kuznetsova, and M. Hoshino, Geophys. Res. Lett. **29**, 2001GL014714 (2002).
[16]L. Yin and D. Winske, Phys. Plasmas **10**, 1595 (2003).
[17]J. U. Brackbill and D. W. Forslund, in *Multiple Times Scales*, edited by J. U. Brackbill and B. I. Cohen (Academic, Orlando, 1985) p. 271.
[18]P. Ricci, G. Lapenta, and J. U. Brackbill, J. Comput. Phys. **183**, 117 (2002).
[19]H. X. Vu and J. U. Brackbill, Comput. Phys. Commun. **69**, 253 (1992).
[20]D. Forslund, Space Sci. Rev. **42**, 3 (1985).
[21]R. Morse and C. Nielson, Phys. Fluids **14**, 830 (1971).
[22]K. Nishimura, S. P. Gary, H. Li, and S. A. Colgate, Phys. Plasmas **10**, 347 (2003).
[23]N. A. Bobrova, S. V. Bulanov, J. I. Sakai, and D. Sugiyama, Phys. Plasmas **8**, 759 (2001).
[24]J. F. Drake, M. Swisdak, C. Cattell, M. A. Shay, B. N. Rogers, and A. Zeiler, Science **299**, 873 (2003).
[25]E. G. Harris, Nuovo Cimento Soc. Ital. Fis., D **23**, 115 (1962).
[26]G. Lapenta and J. U. Brackbill, Geophys. Res. Lett. **23**, 1713 (1996).
[27]J. Dreher, U. Arendt, and K. Schindler, J. Geophys. Res. **101**, 27375 (1996).
[28]D. W. Forslund, K. B. Quest, J. U. Brackbill, and K. Lee, J. Geophys. Res. **89**, 2142 (1984).
[29]G. Lapenta and J. U. Brackbill, J. Geophys. Res. **102**, 27099 (1997).
[30]G. Lapenta and J. U. Brackbill, Phys. Plasmas **9**, 1544 (2002).
[31]G. Lapenta and J. U. Brackbill, Nonlinear Processes Geophys. **7**, 151 (2000).
[32]G. Lapenta, J. U. Brackbill, and W. Daughton, Phys. Plasmas **10**, 1577 (2003).
[33]P. Ricci, G. Lapenta, and J. U. Brackbill, Geophys. Res. Lett. **31**, L06801, 10.1029/2003GL019207 (2004).
[34]W. Daughton, Phys. Plasmas **9**, 3668 (2002).
[35]W. Daughton, Phys. Plasmas **10**, 3103 (2003).
[36]P. L. Pritchett, IEEE Trans. Plasma Sci. **28**, 1976 (2000).
[37]M. M. Kuznetsova, M. Hesse, and D. Winske, J. Geophys. Res. **105**, 7601 (2000).
[38]P. Ricci, G. Lapenta, and J. U. Brackbill, Phys. Plasmas **10**, 3554 (2003).
[39]M. A. Shay and J. F. Drake, Geophys. Res. Lett. **25**, 3759 (1998).
[40]M. A. Shay, J. F. Drake, B. N. Rogers, and R. E. Denton, J. Geophys. Res. **106**, 3759 (2001).
[41]B. U. O. Sonnerup, in *Solar System Plasma Physics*, edited by L. T. Lanzerotti, C. F. Kennel, and E. N. Parker (North-Holland, New York, 1979), Vol. III, p. 45.
[42]T. Terasawa, Geophys. Res. Lett. **10**, 475 (1983).
[43]X. Wang, A. Bhattacharjee, and Z. W. Ma, J. Geophys. Res. **105**, 27633 (2000).